INTERNATIONAL JOURNAL FOR NUMERICAL METHODS IN FLUIDS
Int. J. Numer. Meth. Fluids 2001; **35**: 281–297

A level set technique applied to unsteady free surface flows

A. Iafrati*[,1], A. Di Mascio and E. F. Campana

Istituto Nazionale per Studi ed Esperienze di Architettura Navale (INSEAN), Via di Vallerano 139, 00128 Rome, Italy

SUMMARY

An unsteady Navier–Stokes solver for incompressible fluid is coupled with a level set approach to describe free surface motions. The two-phase flow of air and water is approximated by the flow of a single fluid whose properties, such as density and viscosity, change across the interface. The free surface location is captured as the zero level of a distance function convected by the flow field. To validate the numerical procedure, two classical two-dimensional free surface problems in hydrodynamics, namely the oscillating flow in a tank and the waves generated by the flow over a bottom bump, are studied in non-breaking conditions, and the results are compared with those obtained with other numerical approaches. To check the capability of the method in dealing with complex free surface configurations, the breaking regime produced by the flow over a high bump is analyzed. The analysis covers the successive stages of the breaking phenomenon: the steep wave evolution, the falling jet, the splash-up and the air entrainment. In all phases, numerical results qualitatively agree with the experimental observations. Finally, to investigate a flow in which viscous effects are relevant, the numerical scheme is applied to study the wavy flow past a submerged hydrofoil. Copyright © 2001 John Wiley & Sons, Ltd.

KEY WORDS: free surface flow; level set; two-phase flow; wave breaking

1. INTRODUCTION

Several important phenomena occurring in naval hydrodynamics, such as wave breaking, cavitation and ventilation, cannot be properly faced with standard numerical techniques. As an example, suitable models based on simplified assumptions [1] are usually employed to prevent the occurrence of complex topological configurations of the air–water interface [2].

Historically, the first attempt to treat flows with complex interface was made by Harlow and Welch [3], who developed the marker and cell (MAC) method. In this method, the interface is reconstructed by following massless interface particles that move with the local fluid velocity.

* Correspondence to: INSEAN, Via di Vallerano 139, 00128 Rome, Italy. Tel.: +39 6 50299296; Fax: +39 6 5070619.
[1] E-mail: a.iafrati@mail.insean.it

Received July 1999
Revised January 2000

This interesting approach, although successively modified and improved by several authors [4,5], has proved to be computationally expensive. Rather than following marker particles, Hirt and Nichols [6] introduced the volume of fluid (VOF) approach in which a marker function, the void fraction, is transported by the flow to describe the interface motion.

Recently, approaches that describe the two-phase flow of immiscible fluids have been developed: some are essentially based on a VOF approach [7,8], whereas others are based on the level set (LS) technique [9,10]. In both cases, the two-phase flow is approximated by the flow of a single fluid whose physical properties, namely density and viscosity, vary across the interface. If compressible effects can be neglected in the two phases, the distribution of fluid properties in the whole domain is only related to the interface motion. Hence, besides the integration of the fluid dynamic equations, a transport equation for an additional variable locating the interface is solved. In doing that, particular attention is devoted to keep the transition zone of the fluid properties as narrow as possible.

In the VOF approach, the additional variable is the volume concentration and local fluid properties are expressed as a weighted average of the properties of the fluids, by using the volume concentration as a weight function. The volume concentration is convected with the flow by integrating the corresponding transport equation. This kind of approach has been used by Muzaferjia *et al.* [11] and by Azcueta *et al.* [12], showing that the method is very efficient in dealing with complex free surface configurations. However, due to the jump of the additional variable at the interface, special care must be posed in the numerical treatment of its transport equation to keep the interface sharp.

In the LS technique, the fluid density and viscosity are expressed as a smooth function of the distance from the interface. The jump in fluid properties is spread in a small neighborhood of the interface, whose thickness, related to the cell size, is kept constant in time. The interface location is captured as the zero contour of a scalar function that represents the signed distance from the interface. This function being continuous across the interface, the numerical treatment of its kinematic equation is not difficult. This method has been applied to two-dimensional wave problems by Vogt and Larsson [13], which carefully investigated the effect of the involved parameters on the numerical solution. The good agreement with experimental data validates the numerical technique.

In this paper, the LS technique is coupled with a finite difference Navier–Stokes solver for an incompressible fluid and the method is applied to study several kinds of unsteady free surface flows. The governing fluid dynamics equations, written in curvilinear co-ordinates, are solved in the whole domain with a fractional step procedure, following the scheme suggested by Zang *et al.* [14] and modified to account for variable density and viscosity. Turbulence and surface tension effects are not included at this stage of the development.

One of the critical items of the LS procedure concerns the re-initialization of the distance function in order to keep constant the thickness of the transition zone. In Reference [10] this is done in a very efficient way, without the need for reconstructing the interface location at each time step, with a great advantage in terms of computational effort, which may become crucial when considering three-dimensional applications. However, with the present paper being mainly concerned with two-dimensional problems, the interface location is reconstructed and the distance function is re-initialized at each time step, leading to a simple numerical procedure.

The method is applied to solve some two-dimensional free surface problems. The standing wave of a fluid in a tank and the wave system generated behind a bump starting impulsively from rest are studied. The results are compared with those obtained by solving the corresponding inviscid flow via moving grid approaches. Next, the flow over a high bump, leading to a wave breaking, is analyzed to assess the capability of the numerical method to deal with complex free surface configurations. The method is finally applied to simulate the wavy flow generated past a submerged hydrofoil.

2. THE NAVIER–STOKES SOLVER FOR THE TWO-PHASE FLOW

The two-phase flow is approximated by the flow of a single fluid whose properties change smoothly across the air–water interface. If compressibility effects can be neglected, fluid density and viscosity are simply convected by the flow field. Due to the interface kinematics, the spatial distribution of the fluid properties varies with time. The dimensionless Navier–Stokes equations, in curvilinear co-ordinates, for an incompressible fluid with variable density and viscosity are

$$\frac{\partial U_m}{\partial \xi_m} = 0 \tag{1}$$

$$\frac{\partial}{\partial t}(J^{-1}u_i) + \frac{\partial}{\partial \xi_m}(U_m u_i) = -\frac{1}{\varrho}\frac{\partial}{\partial \xi_m}\left(J^{-1}\frac{\partial \xi_m}{\partial x_i}p\right) - J^{-1}\frac{\delta_{i2}}{Fr^2} + \frac{1}{Re\,\varrho}\frac{\partial}{\partial \xi_m}\left(\mu G^{mn}\frac{\partial u_i}{\partial \xi_n}\right) \tag{2}$$

where x_i and u_i are the ith Cartesian co-ordinate and velocity components, p is the pressure, δ_{i2}/Fr^2 is the gravity term, $Fr = U/\sqrt{gL}$ is the Froude number, δ_{ij} is Kronecker's delta. U and L are the reference values for the velocity and the length respectively, whereas fluid density and viscosity are made non-dimensional by using the water values ϱ_w, μ_w; the Reynolds number is defined as $Re = \varrho_w UL/\mu_w$. J^{-1} is the inverse of the Jacobian or the volume of the cell, and

$$U_m = J^{-1}\frac{\partial \xi_m}{\partial x_j}u_j \tag{3}$$

is the volume flux normal to the ξ_m iso-surface. Finally, G^{mn} is the mesh skewness tensor

$$G^{mn} = J^{-1}\frac{\partial \xi_m}{\partial x_j}\frac{\partial \xi_n}{\partial x_j} \tag{4}$$

Surface tension and turbulence modeling are not included at this stage of the development.

The solution of the above equations is obtained with a numerical scheme similar to that described in Zang *et al.* [14], with only minor adjustments related to the use of variable fluid properties. Cartesian velocities and pressure are defined at the cell center, whereas volume fluxes are defined at the mid-point of the cell faces, where velocities are computed through a quadratic upwind interpolation (QUICK). In this way, the volume flux is conserved on each

control volume and the momentum equation can be written in conservative form. A semi-implicit scheme is adopted for the integration in time of Equation (2). The explicit terms are computed with the Adam–Bashfort scheme, while a Crank–Nicolson discretization is employed for the implicit terms. Since the grid does not depend on time, the discretized form of the momentum equation is

$$J^{-1}(u_i^{n+1}-u_i^n)=\Delta t\left\{\left(1+\frac{\Delta t}{2\Delta t_p}\right)\left[C_i^n+\frac{1}{Re\,\varrho}D_E(u_i^n)\right]-\frac{\Delta t}{2\,\Delta t_p}\left[C_i^{n-1}+\frac{1}{Re\,\varrho}D_E(u_i^{n-1})\right]\right.$$
$$\left.+\frac{1}{\varrho}R_i(p^{n+1})-J^{-1}\frac{\delta_{i2}}{Fr^2}+\frac{1}{2Re\,\varrho}D_I(u_i^{n+1}+u_i^n)\right\} \tag{5}$$

where $\Delta t=t^{n+1}-t^n$ and $\Delta t_p=t^n-t^{n-1}$; C_i^n represents the convective terms at the time step n, R_i is the gradient operator in curvilinear co-ordinates; D_I and D_E are the diagonal and off-diagonal diffusive operators respectively.

Due to the explicit scheme adopted for the convective terms, the time integration step must be bounded. To this aim, it is chosen at each iteration so that the maximum of the quantity

$$\mathrm{CFL}=\left(\frac{|u|}{\Delta x}+\frac{|v|}{\Delta y}+\frac{|w|}{\Delta z}\right)\Delta t=(|U|+|V|+|W|)\frac{\Delta t}{J^{-1}}$$

in the whole computational domain is constant in time and equal to 0.8 in all the numerical simulations here reported, where CFL is the Courant–Friedrich–Lewy number.

A fractional step approach is adopted to solve Equation (5). Since the pressure field at the new time step is unknown, an auxiliary velocity field u_i^* is introduced and the problem is split into two sub-steps

$$\left(I-\frac{\Delta t}{2Re\,\varrho J^{-1}}D_I\right)(u_i^*-u_i^n)=\frac{\Delta t}{J^{-1}}\left\{\left(1+\frac{\Delta t}{2\,\Delta t_p}\right)\left[C_i^n+\frac{1}{Re\,\varrho}D_E(u_i^n)\right]\right.$$
$$\left.+\frac{\Delta t}{2\,\Delta t_p}\left[C_i^{n-1}+\frac{1}{Re\,\varrho}D_E(u_i^{n-1})\right]+\frac{1}{Re\,\varrho}D_I(u_i^n)-J^{-1}\frac{\delta_{i2}}{Fr^2}\right\} \tag{6}$$

$$\left(I-\frac{\Delta t}{2Re\,\varrho J^{-1}}D_I\right)(u_i^{n+1}-u_i^*)=\Delta t\frac{1}{\varrho J^{-1}}R_i(p^{n+1}) \tag{7}$$

Equation (6) is solved to determine the auxiliary velocity field u_i^* (*predictor step*), whereas, in Equation (7), it is assumed that the velocity field u_i^{n+1} is related to the auxiliary one by the following relation (*corrector step*):

$$u_i^{n+1}-u_i^*=\frac{\Delta t}{\varrho J^{-1}}R_i(\phi^{n+1}) \tag{8}$$

By substituting Equation (8) into Equation (7), it can be easily seen that

$$R_i(p^{n+1}) = \varrho\left(J^{-1} - \frac{\Delta t}{2Re} D_I\right)\left(\frac{R_i(\phi^{n+1})}{\varrho J^{-1}}\right) \tag{9}$$

Thus, once the scalar function ϕ is computed, the above relation can be used to calculate the pressure field. In order to save CPU time, as suggested by Rosenfeld *et al.* [15] it can be assumed that $p^{n+1} = \phi^{n+1} + O(\Delta t^2)$.

The corrector function ϕ is determined by enforcing the continuity equation. From Equation (8)

$$u_i^{n+1} = u_i^* + \frac{\Delta t}{\varrho}\left(-\frac{\partial \xi_m}{\partial x_i}\frac{\partial \phi^{n+1}}{\partial \xi_m}\right)$$

and by the definition of fluxes (3)

$$U_m^{n+1} = U_m^* - \frac{\Delta t}{\varrho}\left(G^{ml}\frac{\partial \phi^{n+1}}{\partial \xi_l}\right) \tag{10}$$

Since Cartesian velocity components are defined at the cell centers, a quadratic upwind interpolation is used to reconstruct the auxiliary fluxes at the cell faces. Using the above expression in the continuity equation (1), a Poisson equation for the corrector ϕ is obtained

$$\frac{\partial}{\partial \xi_m}\left(\frac{G^{ml}}{\varrho}\frac{\partial \phi^{n+1}}{\partial \xi_l}\right) = \frac{1}{\Delta t}\frac{\partial U_m^*}{\partial \xi_m} \tag{11}$$

If the velocity is assigned at the boundaries, Equation (10) yields a Neumann boundary condition for Equation (11).

3. KINEMATICS OF THE AIR–WATER INTERFACE

To close the system of differential equations, two transport equations for density and viscosity should be considered

$$\frac{\partial \varrho}{\partial t} + \boldsymbol{u}\cdot\nabla\varrho = 0, \qquad \frac{\partial \mu}{\partial t} + \boldsymbol{u}\cdot\nabla\mu = 0$$

Due to the jump of fluid properties at the interface, the integration of these equations is not straightforward. In the LS technique, this problem is overcome by assuming the fluid properties as smooth functions of the signed normal distance d from the interface. The distance d can be computed for each grid point at $t = 0$, the free surface location being given. It is assumed $d > 0$ in water and $d < 0$ in air. During the time evolution, d can be seen as a property convected by the flow

$$\frac{\partial d}{\partial t} + \boldsymbol{u}\cdot\nabla d = 0 \tag{12}$$

The interface being a material surface, it is always identified with the level $d = 0$.

The smoothing of the jump of fluid properties is achieved by spreading the jump on a small neighborhood of the interface whose thickness, related to the cell size, is kept constant in time [10,16]. Hence, fluid properties are assumed to vary with the distance as follows:

$$f(d) = \begin{cases} f_{\mathrm{w}} & \text{if } d > \delta \\ f_{\mathrm{a}} & \text{if } d < -\delta \\ (f_{\mathrm{w}} + f_{\mathrm{a}})/2 + (f_{\mathrm{w}} - f_{\mathrm{a}})/2 \sin(\pi d/2\delta) & \text{otherwise} \end{cases}$$

δ being the half width of the region along which the jump is spread. In the computation, the thickness δ is chosen so that the jump covers at least three cells in the direction normal to the interface.

Actually, the integration of Equation (12) does not ensure that the thickness of the jump region is kept constant in space and time. To avoid the spreading or concentration of the transition zone, the distance function is re-initialized at each time step as the normal distance from the actual interface. Several schemes have been developed to this aim [17,18]. For instance, this can be done by iterating to steady state the equation

$$\frac{\partial d}{\partial \tau} = S(d)(1 - |\nabla d|) \tag{13}$$

where $S(d)$ is a sign function that is zero on the interface. This procedure, although requiring suitable numerical schemes, is very efficient since it avoids the reconstruction of the interface at each time step [10], which, for three-dimensional problems, is computationally expensive.

However, with this work being concerned only with two-dimensional flows, the reconstruction is not too heavy. Thus, at each time step the interface is found by locating the position of the level $d = 0$ and the distance function $d(x, t)$ is recomputed at each cell center. This simplified procedure is found effective in terms of mass conservation and in dealing with flows characterized by complex interface topologies.

4. NUMERICAL RESULTS

The developed numerical method is applied to simulate several kinds of unsteady free surface flows, ranging from simple to complex interface topologies. In the first application, a simple test case is used to evaluate the converge properties of the scheme. Next, the wavy flow over a bump is studied in both breaking and non-breaking regime. Finally, the method is applied to study the wavy flow past a submerged hydrofoil.

4.1. Oscillating flow in a tank

In this first test, the oscillating flow in a tank is studied. This problem allows us to evaluate the capabilities of the numerical method to describe free surface dynamics and to preserve mass. Results are then compared with those obtained by Lilek [19] for an inviscid fluid.

The tank extends horizontally from $x = -0.5$ to $x = 0.5$ and from $y = 0$ to $y = 1.4$ in the vertical direction. The free surface elevation at $t = 0$ is

$$y(x) = 1 - 0.01 \sin(\pi x)$$

so that the height of the interface over the bottom is $h_l(0) = 1.01$ on the left wall and $h_r(0) = 0.99$ on the right one. For this flow, $U = \sqrt{gL}$ is assumed as a reference value for the velocity, so that the Froude number is $Fr = 1$. The Reynolds number is $Re = 10^6$ and the following values are used for density and dynamic viscosity in air:

$$\varrho_a/\varrho_w = 0.00125, \qquad \mu_a/\mu_w = 18 \times 10^{-3}$$

To evaluate the grid sensitivity, three grids are used: the coarse one has 20 equally spaced cells in the horizontal direction and 140 cells in the vertical direction, suitably clustered close to the free surface region. In particular, in the region $y \in (0.985, 1.015)$, a uniform vertical spacing $\Delta y = 0.0005$ is adopted. The medium and fine grids are obtained by halving the cell size in both directions. The width of the jump region is fixed in order to cover eight grid cells, being $\delta = 0.002$ for the coarse grid, $\delta = 0.001$ for the medium grid and $\delta = 0.0005$ for the finest one.

Figure 1 shows the time histories of the free surface height on the left wall of the tank for different grid resolutions and the inviscid result obtained by Lilek [Personal Communications, 1999]. In the plot, the curve at $d = 0$ is chosen to represent the free surface location obtained with the LS technique. As expected, a fine resolution is required to avoid an excessive damping of the free surface height.

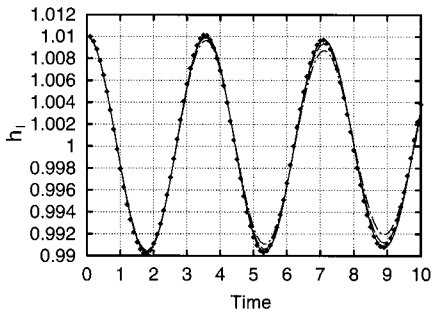

Figure 1. Time histories of the free surface height on the left wall of the tank: (diamonds) Lilek; (dash-dotted) 20×140; (dashed) 40×280; (solid) 80×560.

As a measure of the mass conservation, the ratio between the variation of the mean free surface height $h_m(t)$ with respect to its initial value $h_m(0) = 1$ and the maximum free surface displacement $h_l(0) - h_m(0) = 0.01$, is chosen. In Figure 2, the time histories of this parameter for different grid resolutions are reported; as expected, the better conservation is achieved for the finer grid.

Besides grid sensitivity, this test is also used to investigate the role of the width of the jump region while keeping fixed the computational grid. For the medium grid, computations are performed by using also $\delta = 0.0005$ and $\delta = 0.002$, i.e., the jump is spread over 4 and 16 grid cells. It is interesting to note that this parameter does not affect the free surface dynamics (Figure 3), the three curves being practically indistinguishable, whereas a larger value may have some effects on the mass conservation (Figure 4).

4.2. Flow over a bump: non-breaking regime

In the second application, the flow over a bump in a non-breaking regime is simulated, and the results are compared with those obtained by solving the corresponding potential flow problem

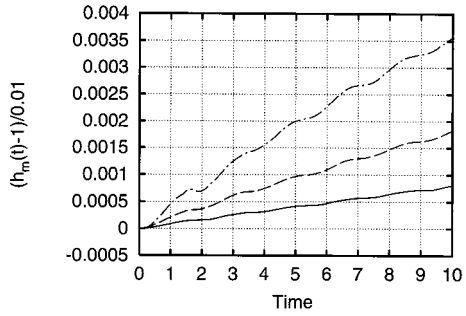

Figure 2. Effect of the grid resolution on the mass conservation: (dash-dotted) 20×140; (dashed) 40×280; (solid) 80×560.

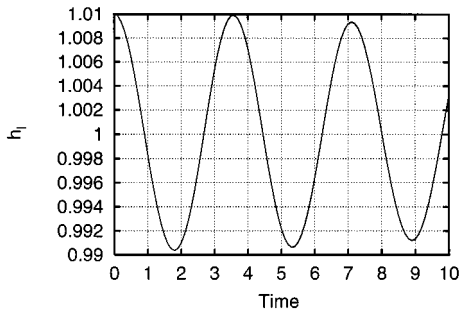

Figure 3. Time histories of the free surface height on the left wall of the tank: (solid) $\delta = 0.0005$; (dashed) $\delta = 0.001$; (dash-dotted) $\delta = 0.002$.

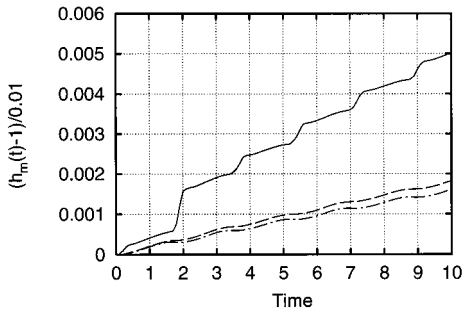

Figure 4. Effect of the width of the jump region on the mass conservation: (solid) $\delta = 0.0005$; (dashed) $\delta = 0.001$; (dash-dotted) $\delta = 0.002$.

through a panel method in order to assess the capability of the numerical procedure to correctly model the wave dynamics. The bump is placed on the bottom of a channel with a still water level $h = 1$ and has a geometric profile

$$y(x) = \begin{cases} 0 & |x| > a \\ -1 + d\left(1 - 2\dfrac{x^2}{a^2} + \dfrac{x^4}{a^4}\right) & x \in (-a, a) \end{cases} \tag{14}$$

d being the maximum height of the bump. At $t = 0$, the bump is suddenly started at $U = 1$ and $Fr = 0.707$; the resulting wavy flow is studied in a frame of reference moving with the bump. In the computations, $d = 0.1$ and $a = 0.5$ are chosen. The computational domain extends from $x = -14$ to $x = 14$ horizontally and from the bottom profile (14) to $y = 0.4$ vertically.

Both in the LS approach and in the panel method, numerical beaches [13,20] are employed to damp out outgoing waves at the computational boundaries. In particular, for the LS the transport equation of the distance function is modified as follows:

$$\frac{\partial d}{\partial t} = -\boldsymbol{u} \cdot \nabla d - \gamma(y + d)$$

where γ is a damping coefficient that grows quadratically from zero to a given value at the outer boundaries. In the above simulations, $\gamma \neq 0$ when $x \in (-14, -8)$ and $x \in (8, 14)$; the limit value is $\gamma = 2$. In order to have a fair comparison, free slip boundary conditions are used at the top and bottom boundaries.

For the computation with the LS, a grid with 220×71 cells is used. Cells are clustered around the bump in the horizontal direction, whereas a uniform vertical spacing $\Delta y = 0.01$ is used for $y \in (-0.2, 0.2)$. The width of the jump region is fixed as $\delta = 0.03$. About 240 elements are employed to discretize the free surface in the panel method.

In Figure 5, the free surface profiles obtained by the LS and by the panel method at $t = 24$ are shown. The comparison exhibits an excellent agreement, confirming that the LS method mirrors the wave dynamics given by the panel method. As it can be observed in Figure 6, when the simulation proceed further on, some discrepancy occurs, probably in consequence of the different beach models employed in the two approaches.

In Figure 7, the velocity field in air and water along a wave period is shown together with two enlarged views close to a crest and a trough. The stripes represent the variable density region while, for the sake of clarity, velocities are plotted at every other grid point and the uniform velocity $(u, v) = (1, 0)$ is subtracted from the local velocity vector to emphasize the local behavior.

It is interesting to note the coupled behavior of the velocity field in the two fluids. According to the classical theory of water waves, near the crests the water moves in the same direction of the wave while near the troughs it moves back. At the same time the flow in air shows an opposite behavior with respect to the flow in water.

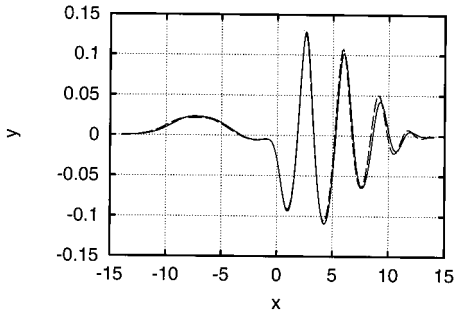

Figure 5. Comparison between free surface profiles obtained by LS (solid line) and panel method (dashed line) at $t = 24$.

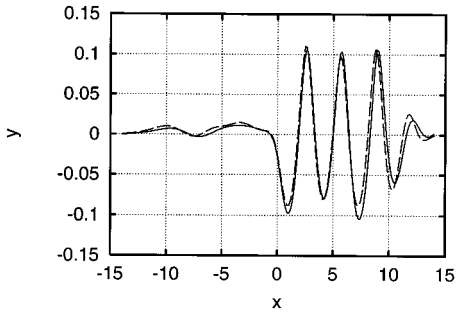

Figure 6. Comparison between free surface profiles obtained by LS (solid line) and panel method (dashed line) at $t = 150$.

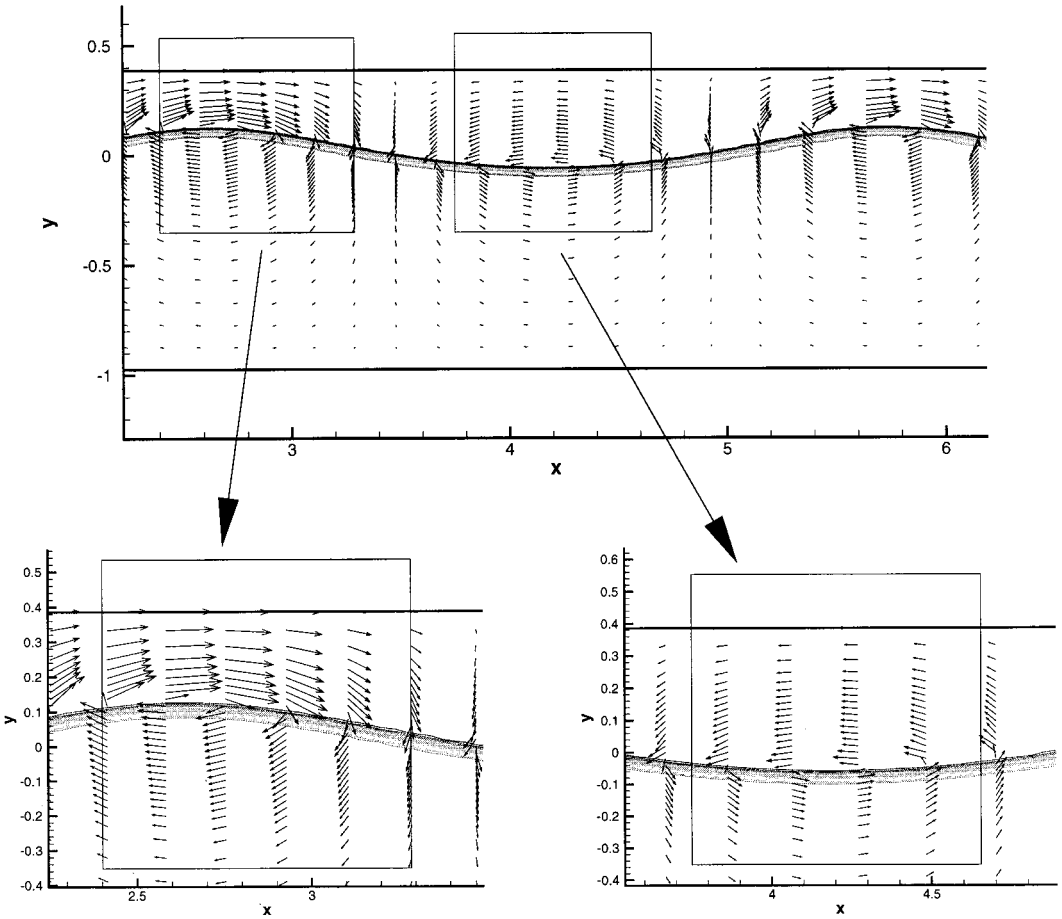

Figure 7. Velocity field in air and water. For the sake of clarity velocities are plotted every second grid point and the uniform horizontal velocity is subtracted from the local value.

4.3. Flow over a bump: breaking regime

It may be observed that the results presented so far could be more efficiently achieved with other numerical techniques; of course, the aim of these numerical tests was to check the properties of the LS method before applying it to more complicated problems.

Since the method is developed to deal with complex air–water interface, the flow over a large bump, leading to wave breaking, is analyzed. In this case, the bump extends from $x = -1$ to $x = 1$ and has a maximum height of $d = 0.4$. For these conditions, the panel method predicts the occurrence of breaking at $t \simeq 3.6$.

In order to describe the different phases characterizing the breaking phenomenon, namely the steep wave formation, the jet development, the splash-up and the entrainment of air, the grid is refined for $x \in (0, 5)$. Moreover, the computational domain is enlarged in the vertical direction up to $y = 1.6$ because of the expected high crest behind the bump. The complete grid used in the simulations is 537×130. Simulations are carried out at $Re = 10^4$ and $\mu_a/\mu_w = 18 \times 10^{-3}$.

In Figure 8, the free surface profiles obtained at $t = 3.6$ by the panel method and by the LS are compared; despite the steep wave, a good agreement between the two solutions is observed. In the simulation with the LS, some numerical instabilities on the free surface develop close to the first trough and propagate downstream. These are probably related to the insufficient spatial resolution of the viscous terms.

The inviscid simulation, because of the algorithm adopted, is not able to proceed beyond the breaking onset. In contrast, the LS simulation is performed well beyond the wave breaking and several splash-up formations are observed. In Figure 9 free surface profiles are plotted with time step $\Delta t = 0.2$ from $t = 4.2$ up to $t = 5.8$. In Figure 10, profiles are plotted with time step $\Delta t = 0.5$ from $t = 6.5$ up to $t = 8.5$.

It can be noticed that from $t = 4.2$ to $t = 5$, the first wave crest behind the bump is increasing in size and steepness. Due to the velocity field induced by this process, a first jet develops at $t \simeq 5$ but its edge breaks into bubbles that are numerically dissipated before impacting the water. The same effect occurs also later as it can be observed at $t = 5.8$. In this case, however, the bubble is larger and falls onto the free surface before being dissipated. Numerical diffusion can be also responsible for the damping of the slight free surface oscillations that are evident at $t = 5.4$ and $t = 5.6$ at the wave crest and that disappear later.

After $t = 6$, the jet is sufficiently developed so that it impacts the free surface before $t = 6.5$. The impact of the jet on the free surface lead to an air entrainment and also to a splash-up just ahead of the impact point onto the free surface. As experimentally observed [21], this splash-up evolves and eventually its forward face impacts again on the free surface at $t \in (7.5, 8)$, leading to another air entrainment and another splash-up process. This second splash-up jet impacts on the free surface at $t \in (8, 8.5)$ and the process proceeds in the same way as before, even though the splash-up intensity gradually decreases.

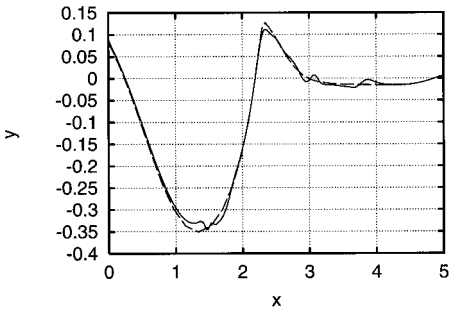

Figure 8. Comparison between free surface profiles obtained by LS (solid line) and panel method (dashed line) at $t = 3.6$.

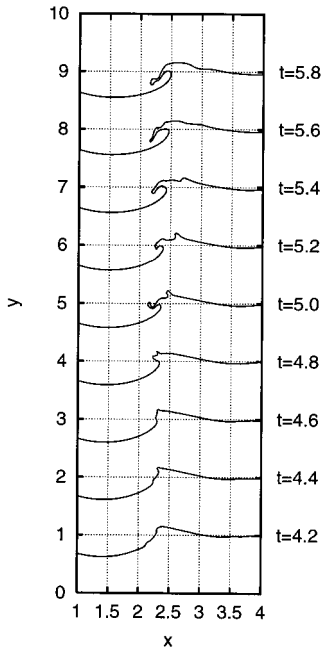

Figure 9. Several configurations of the free surface showing the jet development. A vertical shift $\Delta y = 1$ is applied between two successive configurations. ($t = 4.2 \rightarrow 5.8$, step 0.2).

Although a quantitative comparison is not established, the dynamics described are in qualitative agreement with the experimental observation discussed by Bonmarin [21]. He found that, depending on the flow conditions, after the first splash-up the flow can either degenerate into a chaotic motion or into successive splash-up cycles, as it seems to be the case for the present simulation.

In Figure 11, the velocity field in air and water at the instant when the jet hits the free surface is shown. For the sake of clarity, velocity vectors are displayed at every third grid point in both directions and the uniform horizontal velocity is subtracted from the local value to emphasize the local behavior. Due to the jet impingement, an intense flow is induced in air, leading to the formation of two counter rotating vortices immediately ahead of the impact point. In water, the flow toward the jet and also the strong backward velocity that occurs below the trough up to the head of the breaker can be observed. Also this effect was confirmed experimentally [22].

4.4. Flow past a submerged hydrofoil

The above applications are carried out essentially for validating the capability of the numerical approach in describing the dynamics of the free surface, even when complex topologies of the interface are involved. Since comparisons were established with inviscid numerical solutions, only inertial-dominated flows were considered.

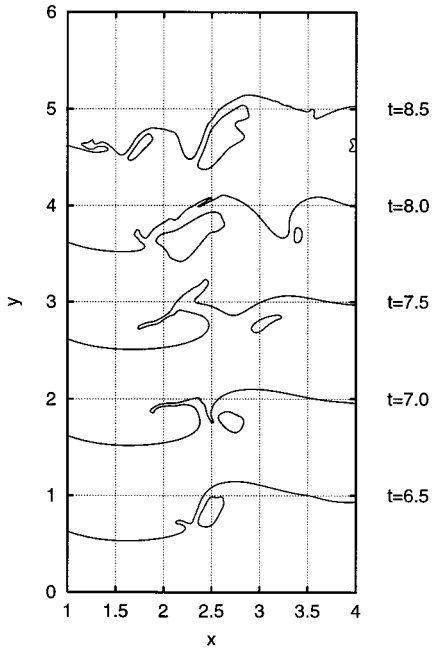

Figure 10. Several configurations of the free surface showing successive splash-up processes ($t = 6.5 \rightarrow 8.5$, step 0.5).

As an example of a problem where viscous effects play a significant role, the wavy flow generated behind an inclined hydrofoil, moving beneath the free surface, is shown in Figure 12. The solid body is modeled via a body forces approach [23].

The hydrofoil is an NACA 0012, 5° angle of attack and the depth at the quarter of chord is 1.034. Numerical simulations are performed with $Re = 10^4$ and $Fr = 0.567$. In Figure 12, the vorticity contours in the whole domain are shown; the shear layer near $y = 0$ represents the free surface. Due to the moderate Reynolds number, an unsteady separation from the suction side occurs; it may be interesting to note that the dipole structures shedded behind the hydrofoil, which rise up and interact with the free surface. Verification and validation of these kind of flows will be the subject of a future work.

5. CONCLUSIONS

In the present paper an LS approach is used to investigate several unsteady two-dimensional free surface flows. A finite difference Navier–Stokes solver in curvilinear co-ordinates is used in conjunction with the LS technique to compute the flow field both in air and water.

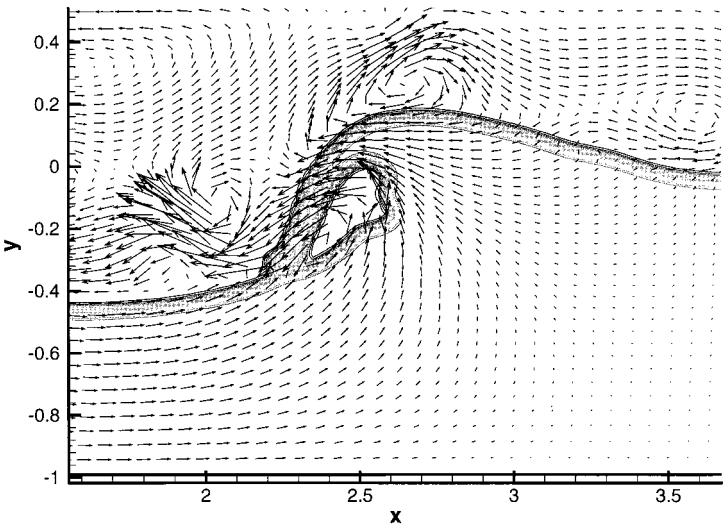

Figure 11. Velocity field in air and water at the jet impingement ($t = 6.3$). For the sake of clarity, velocities are plotted every third grid point and, to emphasize the local behavior, the uniform horizontal velocity is subtracted from the local value.

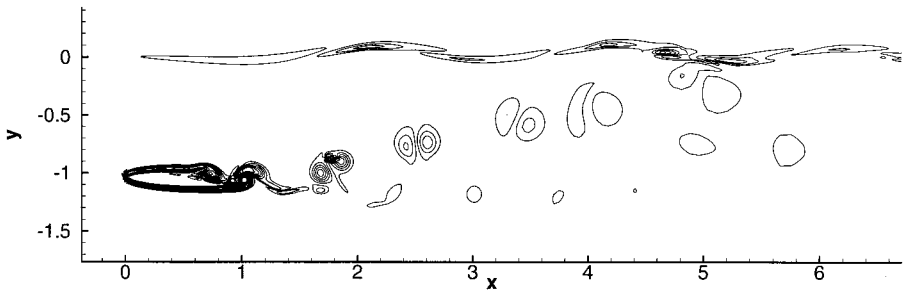

Figure 12. Vorticity contours for the flow about a submerged hydrofoil. Contours about $y = 0$ represent the shear layer at the interface.

The method is applied to the analysis of three classical hydrodynamic problems, namely the oscillating flow in a tank, the wave system generated behind a bump moving in a channel and the wavy flow generated by the motion of a submerged hydrofoil. The numerical method shows its capability in simulating different free surface problems and in dealing with complex interface shapes. For the all analyzed flows, results agree satisfactorily with experimental observations.

In the simulation of the two-dimensional wavy flow past a submerged hydrofoil, due to the moderate Reynolds number, an intense flow separation from the suction side occurs, and vorticity structures, released by the hydrofoil, rise up and strongly interacts with the free surface downstream.

From the numerical point of view, several improvements may be pursed. The most important concerns the turbulence modeling and surface tension effects, that will be included in the method in the sequel of the research.

ACKNOWLEDGMENTS

This work was supported by the Ministero dei Trasporti e della Navigazione in the frame of INSEAN research plan 1997–1999.

REFERENCES

1. Cointe R, Tulin M. A theory of steady breakers. *Journal of Fluid Mechanics* 1994; **276**: 1–20.
2. Banner ML, Peregrine DH. Wave breaking in deep water. *Annual Review in Fluid Mechanics* 1993; **25**: 373–397.
3. Harlow FH, Welch JE. Numerical calculation of time dependent viscous incompressible flow with free surface. *Physics of Fluids* 1965; **8**: 2182–2189.
4. Daly JD. A technique for including surface tension effects in hydrodynamic calculations. *Journal of Computational Physics* 1969; **4**: 97–117.
5. Chen S, Johnson DB, Raad PE. Velocity boundary conditions for the simulation of free surface fluid flow. *Journal of Computational Physics* 1995; **116**: 262–276.
6. Hirt CW, Nichols BD. Volume of fluid (VOF) method for dynamics of free boundaries. *Journal of Computational Physics* 1981; **39**: 201–221.
7. Lafaurie B, Nardone C, Scardovelli R, Zaleski S, Zanetti G. Modelling merging and fragmentation in multiphase flows with SURFER. *Journal of Computational Physics* 1994; **113**: 134–147.
8. Muzaferija S, Peric M. Computation of free surface flows using interface-tracking and interface-capturing methods. In *Nonlinear Water Wave Interaction*, Mahrenholtz O, Markiewicz M (eds). Computational Mechanics Publications: Southampton, UK, 1998.
9. Osher S, Sethian JA. Fronts propagating with curvature-dependent speed: algorithms based on Hamilton–Jacobi formulations. *Journal of Computational Physics* 1988; **79**: 12–49.
10. Sussman M, Smereka P, Osher S. A level-set approach for computing solutions to incompressible two-phase flow. *Journal of Computational Physics* 1994; **114**: 146–159.
11. Muzaferija S, Peric M, Sames P, Schellin T. A two-fluid Navier–Stokes solver to simulate water-entry. In *Proceedings of the 22nd Symposium on Naval Hydrodynamics*, Washington, DC, Rood E (ed.). National Academy Press: Washington, DC, 1998; 638–651.
12. Azcueta R, Muzaferija S, Peric M, Yoo SD. Computation of flows around hydrofoils under the free surface. In *Proceedings of the 7th Conference on Numerical Ship Hydrodynamics*, Nantes, France, vol. 2.7, Piquet J (ed.). National Academy Press: Washington, DC, 1999; 1–10.
13. Vogt M, Larsson L. The level set methods for predicting viscous free surface flows. In *Proceedings of the 7th Conference on Numerical Ship Hydrodynamics*, Nantes, France, vol. 2.4, Piquet J (ed.). National Academy Press: Washington, DC, 1999; 1–19.
14. Zang Y, Street RL, Koseff JR. A non-staggered grid, fractional step method for time-dependent incompressible Navier–Stokes equations in curvilinear coordinates. *Journal of Computational Physics* 1994; **114**: 18–33.
15. Rosenfeld M, Kwak D, Vinokur M. A fractional step solution method for the unsteady incompressible Navier–Stokes equations in generalized coordinate system. *Journal of Computational Physics* 1991; **94**: 102–137.
16. Unverdi SO, Tryggvason G. A front-tracking method for viscous, incompressible, multi-fluid flows. *Journal of Computational Physics* 1992; **100**: 25–37.
17. Adalsteinsson D, Sethian JA. The fast construction of extension velocities in level set methods. *Journal of Computational Physics* 1999; **148**: 2–22.
18. Beux F, Banerjee S. Numerical simulation of three-dimensional two-phase flows by means of a level set method. In *Proceedings of the 3rd ECCOMAS Conference*, Paris, France. Wiley, 1996; 563–569.
19. Ferziger JH, Peric M. *Computational method for fluid dynamics*. Springer: Berlin, 1996.

20. Baker GR, Meiron DI, Orszag SA. Generalized vortex methods for free surface flow problems. II: radiating waves. *Journal of Science and Computers* 1989; **4**: 237–259.
21. Bonmarin P. Geometric properties of deep-water breaking waves. *Journal of Fluid Mechanics* 1989; **209**: 405–433.
22. Lin C, Hwung HH. External and internal flow fields of plunging breakers. *Experiments in Fluids* 1992; **12**: 229–237.
23. Iafrati A, Campana EF. A level-set technique applied to complex free surface flows. In *Proceedings of ASME FEDSM'00—Fluid Engineering Division Summer Meeting*, Boston, MA; FEDSM2000/11257. ASME, 2000.